

Pinch-line spin liquids as layered Coulomb phases

N. Davier,^{1,*} F. A. Gómez Albarracín,^{2,3,†} H. Diego Rosales,^{2,3,‡} P. Pujol,^{4,§} and Ludovic D.C. Jaubert^{1,¶}

¹*CNRS, Université de Bordeaux, LOMA, UMR 5798, 33400 Talence, France*

²*Instituto de Física de Líquidos y Sistemas Biológicos, CONICET,*

Facultad de Ciencias Exactas, Universidad Nacional de La Plata, 1900 La Plata, Argentina

³*Departamento de Ciencias Básicas, Facultad de Ingeniería, UNLP, La Plata, Argentina*

⁴*Laboratoire de Physique Théorique, Université de Toulouse, CNRS, UPS, France*

(Dated: February 25, 2025)

Spin liquids form fluctuating magnetic textures which have to obey certain rules imposed by frustration. These rules can often be written in the form of a Gauss law, indicating the local conservation of an emergent electric field. In reciprocal space, these emergent Gauss laws appear as singularities known as pinch points, that are accessible to neutron-scattering measurements. But more exotic forms of electromagnetism have been stabilized in spin liquids, and in a few rare instances, these zero-dimensional singularities have been extended into one-dimensional pinch lines. Here we propose a simple framework for the design of pinch-line spin liquids in a layered structure of two-dimensional algebraic spin liquids. A plethora of models can be build within this framework, as exemplified by two concrete examples where our theory is confirmed by simulations, and where the rank of the tensorial gauge field is continuously varied along the pinch line, opening new avenues in fractonic matter. We conclude our letter with guidelines for experimental realizations.

Spin liquids are the hallmark of frustrated magnetism. Being magnetically disordered, they fail to be characterized by order parameters. This is why alternative descriptions have proven to be necessary, such as topological orders [1] and fractionalized excitations [2, 3], often related to an underlying emergent gauge field theory [4]. Electromagnetism is probably the most natural form of emergent gauge field for spin liquids; frustration induces a microscopic constraint between spins, which can be rewritten as the local conservation rule of an emergent field or, in other words, the zero divergence of Maxwell equations [5]. Such peculiar spin-spin correlations decay algebraically in real space, and take the form of a characteristic singularity in reciprocal space, the so-called pinch point, readily available to neutron-scattering measurements.

The elegance of emergent phenomena is that they are not confined to our natural intuition. Exotic gauge fields can be explored where charges become magnetic [2], quasiparticles are their own antiparticles [3], and electromagnetic fields evolve into a tensor [6]. Higher-rank (tensorial) gauge fields have recently been actively sought after, as sources for fractons, with potential applications in quantum information [7, 8]. Although the first models were somewhat complex [9–11], more realistic Hamiltonians have subsequently been derived [12–15], followed by the theoretical proposals of a plethora of higher-rank spin liquids [16–24], whose tensorial nature transforms the traditional pinch points into multifold ones [25].

There is, however, a family of spin liquids that has remained rare in the literature: the pinch-line spin liquids [12], where the singularity due to the emergent zero divergence forms a line in reciprocal space. As a topological analogy, it is similar to a zero-dimensional monopole becoming a one-dimensional Dirac string. In certain in-

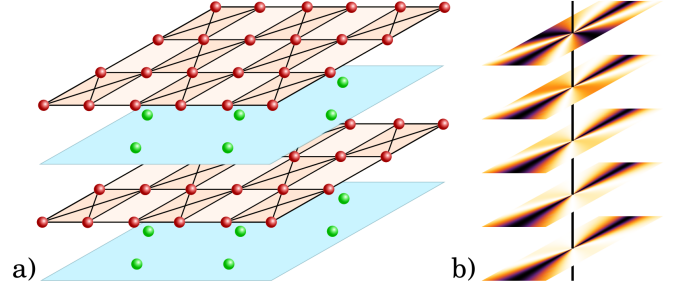


Figure 1. a) Illustration of the pinch-line framework. Planes containing a parent 2D algebraic spin liquid hosting pinch points (depicted as a checkerboard) are placed regularly along a transverse axis, with intermediate layers (in blue) designed to make the pinch points one-dimensional. b) Representation of a pinch line in reciprocal space (black line), with pinch points centered on the line on every transverse plane.

stances, pinch lines can be explained from topological quantum chemistry as a one-dimensional mismatch between two specific band representations of the lattice and Hamiltonian symmetries [21]. First derived in a pyrochlore model in the context of $\text{Tb}_2\text{Ti}_2\text{O}_7$ [12], only a handful of models have been found to support pinch lines so far [12, 16, 20, 21].

In this letter we provide a simple and sufficient, but not necessary, framework to design pinch-line spin liquids. Starting from a two-dimensional (2D) algebraic spin liquid, we explain how to build a 3D model able to continuously propagate pinch-point singularities into parallel lines in reciprocal space. Our method is fairly generic and only relies on standard Heisenberg exchange couplings. As a demonstration of the high degree of model design now achievable in frustrated magnetism, we show how pinch lines can become multifold. Our theory is confirmed by Monte Carlo simulations.

Background – While there is no unique way to stabilize a spin liquid, they are known to naturally occur as the ground state of certain cluster-type Hamiltonians,

$$H = \frac{1}{2} \sum_{\alpha} \mathbf{C}_{\alpha}^2, \quad \mathbf{C}_{\alpha} = \sum_{i \in \alpha} \gamma_i \mathbf{S}_i, \quad (1)$$

with classical Heisenberg spins, where γ_i define the different Heisenberg interactions within cluster α . The pyrochlore and kagome antiferromagnets are famous members of this class of Hamiltonians. The energy of Eq. (1) is minimized by setting the constrainters $\mathbf{C}_{\alpha} = 0, \forall \alpha$ (when possible). Following the Benton-Moessner approach [15], the Fourier transform of $\mathbf{C}_{\alpha} = 0$ gives

$$\sum_{u=1}^n L_u(\mathbf{q}) \tilde{\mathbf{S}}_u(\mathbf{q}) = 0, \quad L_u(\mathbf{q}) = \sum_{j \in D_u} \gamma_j e^{i\mathbf{q} \cdot \mathbf{r}_j}, \quad (2)$$

where u runs over the n inequivalent sublattices, j runs over all sites D_u of sublattice u within the cluster, and \mathbf{r}_j is the position of site j with respect to the cluster center. $\tilde{\mathbf{S}}_u(\mathbf{q})$ is the Fourier transform of the spin configuration on sublattice u . The constraint vector $\mathbf{L}(\mathbf{q}) \equiv \{L_u(\mathbf{q})\}_{u=1, \dots, n}$ encodes most of the spin-liquid properties [15], allowing for a classification of classical spin liquids [18, 19, 21]. In particular, $\mathbf{L}(\mathbf{q}^*) = 0$ indicates the closing of a gap in the energy spectrum, which results in the presence of a pinch point in the structure factor at wave vector \mathbf{q}^* ; it corresponds to an algebraic spin liquid. And in 3D, $\mathbf{L}(\mathbf{q})$ vanishing along an entire line is the signature of a pinch-line spin liquid [20].

The elegance of this formalism is that Eq. (2) can be naturally reformulated as a Gauss law in the vicinity of \mathbf{q}^* [15, 18, 19]. At no loss in generality, let us consider a rank-2 U(1) gauge theory where the Gauss law of the tensor electric field reads $\partial_i \partial_j \tilde{E}_{ij} = 0 \Leftrightarrow q_i q_j \tilde{E}_{ij} = 0$ in Fourier space [6]. The emergent electric field describes the spin degrees of freedom of Eq. (2) [26], while the derivatives of the Gauss law come from the lowest-order expansion of $\mathbf{L}(\mathbf{q}^* + \delta\mathbf{q})$; if the first term of Taylor expansion is second order, then the prefactor in front of \tilde{E}_{ij} is proportional to $q_i q_j$. We then have a rank-2 Gauss law which imposes that some of the correlators of the tensor electric field (e.g. $\langle \tilde{E}_{xx}(\mathbf{q}_{\perp}) \tilde{E}_{yy}(-\mathbf{q}_{\perp}) \rangle$) support a pinch-point singularity with four-fold symmetry [25].

How to design pinch-line models – Let us consider a 2D algebraic spin liquid with n sublattices. This is our parent model with Hamiltonian (1) whose constraint vector $\mathbf{l}(q_x, q_y)$ vanishes at wave vector (q_x^*, q_y^*) . Now, let us stack successive layers of this 2D parent model, inserting intermediate layers as depicted in Fig. 1, with inter-layer distance d . We impose that these intermediate layers form a unique $(n+1)^{\text{th}}$ sublattice; this condition is actually not strictly necessary, but it simplifies the reasoning.

In order to form a 3D structure, these intermediate layers need to interact with the parent layers above and below them. We add these interactions in Hamiltonian (1) via new coefficients δ_i for all clusters α ,

$$\mathbf{C}_{\alpha} = \sum_{i \in \alpha} \left(\gamma_i \mathbf{S}_i^{(p)} + \delta_i \mathbf{S}_i^{(l)} \right), \quad (3)$$

where (p) denotes spins from the 2D parent layers including all sublattices from 1 to n , and (l) represents spins from sublattice $(n+1)$ in the intermediate layers. Based on Eq. (2), the constraint vector $\mathbf{L}(\mathbf{q})$ of the resulting 3D model has $(n+1)$ dimension,

$$\mathbf{L} = \begin{pmatrix} \mathbf{l}(q_x, q_y) \\ L_{n+1}(q_x, q_y, q_z) \end{pmatrix}, \quad (4)$$

with

$$L_{n+1}(\mathbf{q}) = e^{iq_z d} \sum_{j \in D_{n+1}^a} \delta_j e^{i\mathbf{q}_{\perp} \cdot \mathbf{r}_j} + e^{-iq_z d} \sum_{j \in D_{n+1}^b} \delta_j e^{i\mathbf{q}_{\perp} \cdot \mathbf{r}_j}, \quad (5)$$

where $D_{n+1}^{a,b}$ denotes the intermediate layer located either above or below the cluster center, and \mathbf{q}_{\perp} is a shorthand notation for (q_x, q_y) . Since $\mathbf{l}(\mathbf{q}_{\perp})$ does not depend on q_z , the pinch points at \mathbf{q}_{\perp}^* and equivalent wave vectors extend into parallel pinch lines along q_z if $\{L_{n+1}(\mathbf{q}_{\perp}^*, q_z) = 0, \forall q_z\}$. In other words, the necessary condition to form a pinch line in our framework only depends on the positions of, and interactions δ_i with, the intermediate $(n+1)^{\text{th}}$ sublattice:

$$\sum_{j \in D_{n+1}^a} \delta_j e^{i\mathbf{q}_{\perp}^* \cdot \mathbf{r}_j} = 0 = \sum_{j \in D_{n+1}^b} \delta_j e^{i\mathbf{q}_{\perp}^* \cdot \mathbf{r}_j}, \quad (6)$$

Eq. (6) reduces to a single condition if the $(n+1)^{\text{th}}$ sublattice is symmetric with respect to the cluster center, which is natural for most 3D structures. Being one-dimensional in reciprocal space, pinch lines imply a sub-dimensional decoupling of magnetic correlations in real space. In that sense, Eq. (6) can be understood as the necessary balance between intra- and inter-layer couplings to appropriately decouple 2D layers in the zero-energy manifold of a strongly interacting, fully three-dimensional, system.

Multifold pinch lines – We have so far voluntarily remained generic in order to demonstrate the universal breadth of the method. In particular we imposed no condition on the nature of the singularity, and are free to consider multifold pinch points of higher-rank U(1) gauge theories. This freedom raises a follow-up question though: is the multifold symmetry of the parent pinch point preserved along the line? Based on the discussion below Eq. (2), this question can be straightforwardly recast in a mathematical form: do $L_{n+1}(\mathbf{q}_{\perp}, q_z)$ and $\mathbf{l}(\mathbf{q}_{\perp})$ scale at the same lowest order in $\delta\mathbf{q}_{\perp}$ near the singularity, for all q_z ? If yes, the multifold singularity is

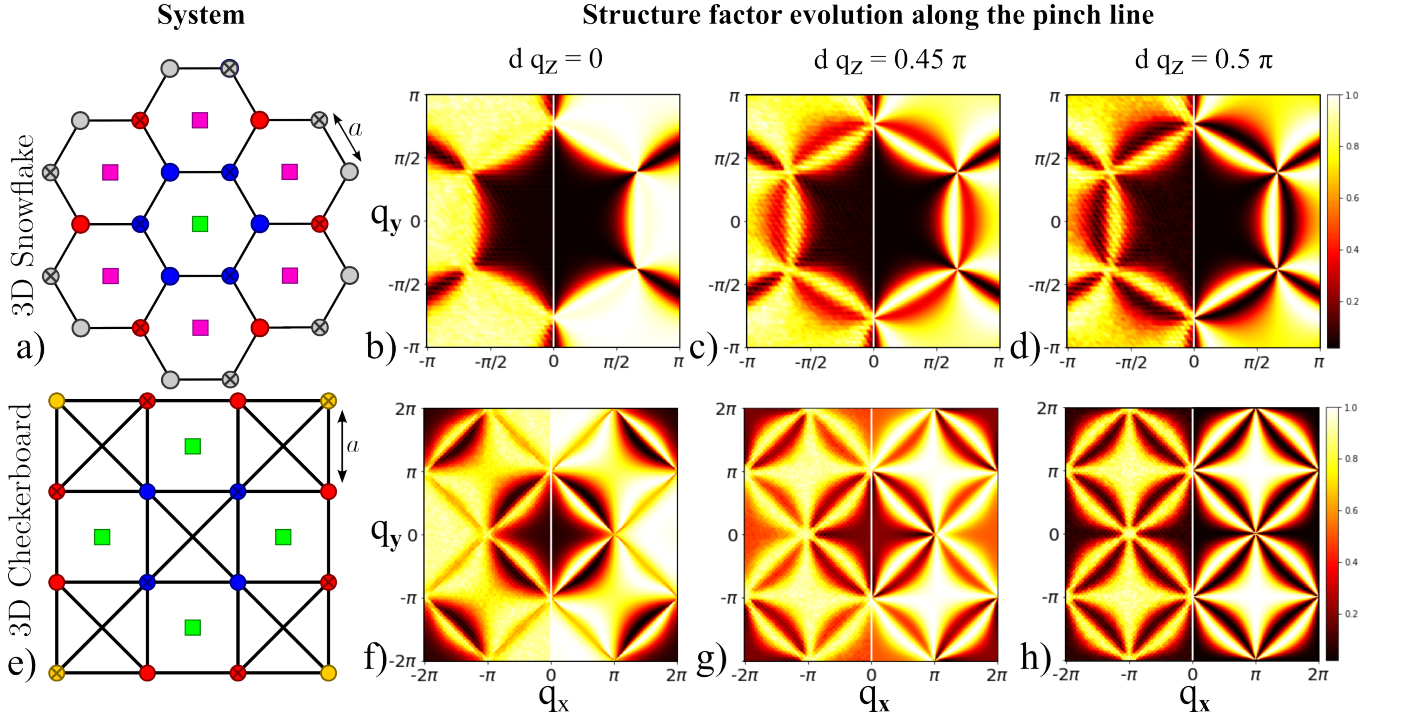


Figure 2. The left panels depict the local cluster structure of the two systems studied here. The plain and crossed circles depict the two sublattices of the 2D parent systems. Blue, red and yellow circles respectively appear with coefficient 1, γ_1 (γ for the snowflake) and γ_2 in the constrainer \mathcal{C} . The squares represent the third sublattice located in intermediate planes; locally, they form square (top) and hexagonal (bottom) bipyramids with the 2D parent lattice. The green and pink squares appear with coefficient δ_1 (δ for the checkerboard) and δ_2 in the constrainer \mathcal{C} . The three right columns show the evolution of the equal-time structure factor in (q_x, q_y) planes orthogonal to the pinch lines (in a^{-1} units), with $\gamma = 1/2, \delta_1 = 1$ for the 3D snowflake and $\gamma_1 = 1, \gamma_2 = -1/3$ and $\delta = 1$ for the 3D checkerboard model. For each panel, the right side is obtained analytically using Henley's projective method [27] [Appendix B], while the left side results from Monte Carlo simulations [Appendix C]. The agreement between simulations and theory is excellent.

conserved. If not, one obtains a mixture of higher-rank gauge fields [18, 20, 22–24]. This condition is actually not as constraining as it might seem. Assuming that all intermediate layers are identical, or at least symmetric with respect to cluster centers, the two sums of Eq. (5) become equal, as we previously explained. The q_z contribution of $L_{n+1}(\mathbf{q}_\perp, q_z)$ thus factorizes out and its Taylor expansion in $\delta \mathbf{q}_\perp$ is automatically the same for all q_z .

Now that the generic framework has been defined, we shall apply our approach to two concrete examples.

The 2D snowflake honeycomb model [15, 20] consists of Hamiltonian (1) with spin clusters

$$\mathcal{C}_\square = \sum_{i \in \square} \mathbf{S}_i + \gamma \sum_{i \in \langle \square \rangle} \mathbf{S}_i \quad (7)$$

defined in Appendix A and illustrated in Fig. 2(a). The ground state of this 2D parent model is known to support an algebraic spin liquid for any $\gamma > 0$ [15]. For $\gamma = 1/2$, this spin liquid evolves into a rank-2 gauge theory with fourfold pinch points at K points in the Brillouin zone (BZ).

There are multiple ways to extend this singularity into a line. We construct a 3D lattice by inserting intermediate triangular layers (see the square sites of Fig. 2(a)). Within each cluster, inter-layer interactions take the form of two additional terms in \mathcal{C}_\square of Eq. (7): sites above and below the respectively central (green) and surrounding (pink) hexagons appear with coefficient δ_1 and δ_2 . The third component of the constraint vector then becomes

$$L_3(\mathbf{q}) = 2\delta_1 \cos(dq_z) \left[1 + \frac{\delta_2}{\delta_1} \sum_{i=1}^6 \cos(\mathbf{r}_i \cdot \mathbf{q}_\perp) \right], \quad (8)$$

where the sum runs over the six pink sites of the cluster [Fig. 2(a)]. Since the fourfold pinch points of the parent model appear at $\mathbf{q}_\perp^K = (0, \frac{4\pi}{3\sqrt{3}a}, 0)$ (and equivalent K points), we get $\{L_3(\mathbf{q}_\perp^K, q_z) = 0, \forall q_z\}$ under the condition

$$1 + \frac{\delta_2}{\delta_1} \sum_{i=1}^6 \cos(\mathbf{r}_i \cdot \mathbf{q}_\perp^K) = 0 \Leftrightarrow \delta_1 = 3\delta_2. \quad (9)$$

Furthermore, Taylor expansion of Eq. (8) gives

$$L_3(\mathbf{q}_\perp^K + \delta \mathbf{q}_\perp, q_z) = 2\delta_2 \cos(dq_z) \frac{3}{4} (\delta q_x^2 + \delta q_y^2) + \mathcal{O}(\delta q_i^3), \quad (10)$$

which is of second order in $\delta\mathbf{q}_\perp$ as, by definition, for the rank-2 parent model. Our model thus supports fourfold pinch lines at $(\mathbf{q}_\perp^K, \forall q_z)$ for $\gamma = 1/2$ and $\delta_1 = 3\delta_2$, with a degree of freedom on the ratio γ/δ_1 !

The tensor electric field \tilde{E}_{2D} of our parent model is traceless, as derived in Ref. [20]. Injecting Eq. (10) into Eq. (2), it can be generalized to our pinch-line spin liquid,

$$\tilde{E}_{3D} = \tilde{E}_{2D} + \eta\tilde{S}_3 \text{Id}_2, \quad (11)$$

where $\eta \propto \delta_2 \cos(dq_z)$ and \tilde{S}_3 is the Fourier transform of the spin configuration on sublattice $u = 3$. The third sublattice makes the scalar charge theory traceful. It breaks the self-duality between electric and magnetic sectors a priori, but preserves charge- and dipole-moment conservation [6]. Our 3D model is thus expected to support fracton excitations.

However, the actual shape of the fourfold singularity in the structure factor $\mathbb{S}(\mathbf{q})$ is subtle. Four-fold pinch points are properly defined in the correlators of the tensor electric field \tilde{E}_{ij} [25] and only appear in some of them (e.g. $\langle \tilde{E}_{xx}(\mathbf{q}_\perp) \tilde{E}_{yy}(-\mathbf{q}_\perp) \rangle$) but not all of them (e.g. not $\langle \tilde{E}_{xx}(\mathbf{q}_\perp) \tilde{E}_{xx}(-\mathbf{q}_\perp) \rangle$). The subtlety is that $\mathbb{S}(\mathbf{q})$ is the Fourier transform of *all* spin-spin correlations, and thus receives contributions from all correlators a priori [27]. This is why multifold pinch points can be somewhat hidden in $\mathbb{S}(\mathbf{q})$. Performing a Taylor expansion in the \mathbf{q}_\perp plane around the pinch line, $\mathbb{S}(\mathbf{q})$ adopts the form

$$\mathbb{S}(\mathbf{q}) \propto \alpha + \beta \frac{q_x^2 q_y^2}{(q_x^2 + q_y^2)^2} + \chi \cos(dq_z) \frac{q_x^4 - q_y^4}{(q_x^2 + q_y^2)^2}, \quad (12)$$

where α , β , and χ are real parameters. This expression is the sum of two terms with distinct symmetries: the term proportional to β exhibits fourfold symmetry, while the term proportional to χ only has twofold symmetry. Both terms are allowed in phases governed by a rank-2 divergenceless tensor E_{ij} [25]. As a consequence, and even though we have a rank-2 gauge theory with a fourfold singularity propagating along the pinch line in the appropriate correlator sectors, the pinch points in the structure factor $\mathbb{S}(\mathbf{q})$ continuously evolve from twofold to fourfold symmetry, as confirmed in Figs. 2(b-d) both analytically and numerically.

The 2D generalized checkerboard model is known to support a diversity of algebraic spin liquids [18]. This diversity offers several pinch points at distinct wave vectors that can be considered as potential pinch lines within our framework. The Hamiltonian of this 2D parent model follows Eq. (1) with spin clusters

$$\mathbf{c}_\square = \sum_{i \in \square} \mathbf{S}_i + \gamma_1 \sum_{i \in \langle \square \rangle} \mathbf{S}_i + \gamma_2 \sum_{i \in \langle\langle \square \rangle\rangle} \mathbf{S}_i, \quad (13)$$

defined in Appendix A and illustrated in Fig. 2(e). We have again several options to build the 3D extension. We

choose to place the third sublattice above (and below) each empty plaquette of the checkerboard lattice (see the squares in Fig. 2(e)), whose sites appear in \mathbf{C}_\square with a unique coefficient δ . In that case, Eq. (5) becomes

$$L_3(\mathbf{q}) = 4\delta \cos(dq_z) [\cos(aq_x) + \cos(aq_y)]. \quad (14)$$

The necessary condition to observe a pinch line, $L_3(\mathbf{q}^*) = 0$, is satisfied for all $q_y = \pm q_x \pm \pi/a$, i.e. for any point on the BZ boundary. Hence, any pinch point of the 2D parent model located on the BZ edge extends into a pinch line in this 3D layered structure. According to Ref. [18], this offers several pinch points from which to choose from. For the sake of originality, we analyzed the Taylor expansion of $L_3(\mathbf{q})$ along the BZ edge; we found that the first-order term vanishes at M points (BZ corners), giving rise to a diagonal traceless rank-2 electric field $\tilde{E}_{xx} = -\tilde{E}_{yy} = 6\delta \cos(q_z d) \tilde{S}_3$. Remarkably, for $\gamma_2 = (1 - 2\gamma_1)/3$, the structure factor of the 2D parent model presents sixfold singularities at M points, attached to a rank-3 field. Hence, we expect in our 3D model an exotic pinch line mixing rank-2 and rank-3 gauge fields, as confirmed in the structure factor of Figs. 2(f-h) both analytically and numerically. Since the rank-2 term disappears when $q_z = \pi/d \pmod{\pi}$, it explains the perfect sixfold symmetry in Fig. 2(h). The rank-3 gauge theory implies the conservation of the charge-, dipole- and quadrupole moments [6, 20], further restricting the movements of emergent fracton excitations.

Discussion – Pinch-line spin liquids form a family of exotic magnetic textures with well-defined one-dimensional singularities in reciprocal space. Very few models have been proposed so far [12, 16, 20, 21]. In this letter, we expose a simple and generic framework to transform most 2D algebraic spin liquids into 3D pinch-line spin liquids. Our theory authorizes a high degree of design and is confirmed numerically on two concrete examples [Fig. 2] which do not order down to the lowest temperatures in Monte Carlo simulations [Appendix C]. In addition to a generic framework, our results open a platform for exotic forms of higher-rank gauge fields, that can continuously evolve along the line in reciprocal space. Consequences on fractonic matter are yet to be explored.

As a next step, our approach is sufficient but not necessary. Extending this framework to other pinch-line models with cubic symmetry and non-parallel pinch lines [12, 16] is appealing. In that context, the topological-quantum-chemistry route recently proposed in Ref. [21] could be beneficial.

As a conclusion, we believe the most promising aspect of our framework is that for each 2D algebraic parent spin liquid, multiple 3D structures are conceivable. Moreover, the choice to consider intermediate layers with only one sublattice was only out of pedagogical convenience; multiple sublattices are perfectly possible,

as long as all $L_{m>n}$ components respect condition (6). Hence, while the cluster form of Hamiltonian (1) imposes constraints on the model, it remains reasonably generic for frustrated magnets. The huge diversity of possible pinch-line models that can be derived in this framework make us hopeful to see some of these models realized in materials in the future, especially since the large entropy of classical spin liquids stabilizes them at finite temperature, even away from fine-tuned model parameters. A subtle, but experimentally relevant, aspect of our theory is that the appearance of the pinch line is independent on the ratio between intra- and inter-layers, since only the latter couplings appear in $L_{n+1}(\mathbf{q})$. It means that the very low-temperature properties of weakly coupled layers, which is a common perturbation to two-dimensional spin liquids, could be a good place to look for pinch lines. Another advantage is that the framework relies on standard isotropic spin-spin Heisenberg exchange terms. There is no need for three- or four-body interactions that are more difficult to realize in experiments. And for materials with strong spin-orbit couplings, nothing prevents to extend our theory to anisotropic interactions, albeit with a more complex form of emergent electric field [14, 22–24, 28, 29]. In the same vein, our theory also applies to Ising and XY spins. Such spin models have a tendency of more easily ordering at low temperature, e.g. via the order-by-disorder mechanism [30] or confinement-deconfinement transitions, which makes 2D parent models a bit less diverse. But recent developments in Rydberg atoms [31–34] offer new avenues to realize such systems experimentally, and motivates to explore the influence of quantum fluctuations on all these pinch-line models.

Acknowledgements – The authors thank the CNRS International Research Project COQSYS for their support. N.D. and L.J. are supported by Grant No. ANR-23-CE30-0038-01. F. A. G. A. and H. D. R. are partially supported by CONICET (PIP 2021-112200200101480CO), SECyT UNLP PI+D X947 and Agencia I+D+i (PICT-2020-SERIE A-03205). F. A. G. A. acknowledges support from PIBAA 2872021010 0698CO (CONICET).

* naimo.davier@u-bordeaux.fr

† albarrac@fisica.unlp.edu.ar

‡ rosales@fisica.unlp.edu.ar

§ pierre.pujol@irsamc.ups-tlse.fr

¶ ludovic.jaubert@u-bordeaux.fr

[1] X.-G. Wen, Phys. Rev. B **65**, 165113 (2002).

[2] C. Castelnovo, R. Moessner, and S. L. Sondhi, Nature **451**, 42 (2008).

[3] A. Kitaev, Annals of Physics **321**, 2 (2006).

[4] J. Knolle and R. Moessner, Annual Review of Condensed Matter Physics **10**, 451 (2019),

<https://doi.org/10.1146/annurev-conmatphys-031218-013401>.

[5] C. L. Henley, Annu. Rev. Condens. Matter Phys. **1**, 179 (2010).

[6] M. Pretko, Phys. Rev. B **96**, 035119 (2017).

[7] M. Pretko, X. Chen, and Y. You, International Journal of Modern Physics A **35**, 2030003 (2020).

[8] R. M. Nandkishore and M. Hermele, Annual Review of Condensed Matter Physics **10**, 295 (2019).

[9] C. Chamon, Phys. Rev. Lett. **94**, 040402 (2005).

[10] C. Xu, Phys. Rev. B **74**, 224433 (2006).

[11] J. Haah, Phys. Rev. A **83**, 042330 (2011).

[12] O. Benton, L. D. C. Jaubert, H. Yan, and N. Shannon, Nature Communications **7**, 11572 (2016).

[13] K. Slagle and Y. B. Kim, Phys. Rev. B **96**, 165106 (2017).

[14] H. Yan, O. Benton, L. D. C. Jaubert, and N. Shannon, Phys. Rev. Lett. **124**, 127203 (2020).

[15] O. Benton and R. Moessner, Phys. Rev. Lett. **127**, 107202 (2021).

[16] N. Niggemann, Y. Iqbal, and J. Reuther, Phys. Rev. Lett. **130**, 196601 (2023).

[17] F. Desrochers, L. E. Chern, and Y. B. Kim, Phys. Rev. B **107**, 064404 (2023).

[18] N. Davier, F. A. Gómez Albarracín, H. D. Rosales, and P. Pujol, Phys. Rev. B **108**, 054408 (2023).

[19] H. Yan, O. Benton, R. Moessner, and A. H. Nevidomskyy, Phys. Rev. B **110**, L020402 (2024).

[20] H. Yan, O. Benton, A. H. Nevidomskyy, and R. Moessner, Phys. Rev. B **109**, 174421 (2024).

[21] Y. Fang, J. Cano, A. H. Nevidomskyy, and H. Yan, Phys. Rev. B **110**, 054421 (2024).

[22] D. Lozano-Gómez, V. Noculak, J. Oitmaa, R. R. P. Singh, Y. Iqbal, J. Reuther, and M. J. P. Gingras, Proceedings of the National Academy of Sciences **121**, e2403487121 (2024), <https://www.pnas.org/doi/pdf/10.1073/pnas.2403487121>.

[23] K. T. K. Chung, Mapping the phase diagram of a frustrated magnet: Degeneracies, flat bands, and canting cycles on the pyrochlore lattice (2024), arXiv:2411.03429 [cond-mat.str-el].

[24] D. Lozano-Gómez, O. Benton, M. J. P. Gingras, and H. Yan, An atlas of classical pyrochlore spin liquids (2024), arXiv:2411.03547 [cond-mat.str-el].

[25] A. Prem, S. Vijay, Y.-Z. Chou, M. Pretko, and R. M. Nandkishore, Phys. Rev. B **98**, 165140 (2018).

[26] Note that there exists a copy of this electric field for each one of the three spin components.

[27] C. L. Henley, Phys. Rev. B **71**, 014424 (2005).

[28] H. Yan, O. Benton, L. Jaubert, and N. Shannon, Phys. Rev. B **95**, 094422 (2017).

[29] K. Essafi, O. Benton, and L. D. C. Jaubert, Phys. Rev. B **96**, 205126 (2017).

[30] R. Moessner and J. T. Chalker, Phys. Rev. B **58**, 12049 (1998).

[31] P. Schauß, J. Zeiher, T. Fukuhara, S. Hild, M. Cheneau, T. Macrì, T. Pohl, I. Bloch, and C. Gross, Science **347**, 1455 (2015), <https://www.science.org/doi/pdf/10.1126/science.1258351>.

[32] P. Scholl, M. Schuler, H. J. Williams, A. A. Eberharter, D. Barredo, K.-N. Schymik, V. Lienhard, L.-P. Henry, T. C. Lang, T. Lahaye, A. M. Läuchli, and A. Browaeys, Nature **595**, 233 (2021).

[33] S. Ebadi, T. T. Wang, H. Levine, A. Keesling, G. Semeghini, A. Omran, D. Bluvstein, R. Samajdar, H. Pich-

- ler, W. W. Ho, S. Choi, S. Sachdev, M. Greiner, V. Vuletić, and M. D. Lukin, *Nature* **595**, 227 (2021).
- [34] C. Chen, G. Bornet, M. Bintz, G. Emperauger, L. Leclerc, V. S. Liu, P. Scholl, D. Barredo, J. Hauschild, S. Chatterjee, M. Schuler, A. M. Läuchli, M. P. Zaletel, T. Lahaye, N. Y. Yao, and A. Browaeys, *Nature* **616**, 691

(2023).

- [35] J. T. Chalker, P. C. W. Holdsworth, and E. F. Shender, *Phys. Rev. Lett.* **68**, 855 (1992).
- [36] M. E. Zhitomirsky, *Phys. Rev. B* **78**, 094423 (2008).

End Matter

Appendix A: Lattice definitions

3D snowflake model – The positions of the 2D snowflake parent model sites that are considered with a coefficient 1 in the constrainer definition (7), and depicted by blue dots on Fig 2(a), are given by

$$\mathbf{r}_{1(4)}^{(p)} = \pm a (1, 0, 0), \quad \mathbf{r}_{2(5)}^{(p)} = \pm a \left(\frac{\sqrt{3}}{2}, \frac{1}{2}, 0 \right),$$

$$\mathbf{r}_{3(6)}^{(p)} = \pm a \left(-\frac{\sqrt{3}}{2}, \frac{1}{2}, 0 \right),$$

while sites taken with a coefficient γ in the constrainer definition, depicted by red dots on Fig 2(a), are sitting at positions

$$\mathbf{r}_{7(10)}^{(p)} = \pm 2a (1, 0, 0), \quad \mathbf{r}_{8(11)}^{(p)} = \pm 2a \left(\frac{\sqrt{3}}{2}, \frac{1}{2}, 0 \right),$$

$$\mathbf{r}_{9(12)}^{(p)} = \pm 2a \left(-\frac{\sqrt{3}}{2}, \frac{1}{2}, 0 \right),$$

For the 3D generalized system, intermediate layers sites, depicted by squares dots on Fig 2(a), are located at positions

$$\mathbf{r}_0^{(l)} = (0, 0, d), \quad \mathbf{r}_{1(4)}^{(l)} = (0, \pm\sqrt{3}a, d),$$

$$\mathbf{r}_{2(5)}^{(l)} = \left(\mp\frac{3}{2}a, \pm\frac{\sqrt{3}}{2}a, d \right), \quad \mathbf{r}_{3(6)}^{(l)} = \left(\mp\frac{3}{2}a, \mp\frac{\sqrt{3}}{2}a, d \right)$$

for the layer located above the 2D parent system plane (and with $-d$ as last component for sites located in the intermediate plane located below).

3D generalized checkerboard model – The positions of the 2D parent sites that are taken with a coefficient 1 in the constrainer definition (13), and depicted as blue dots on Fig 2(e) are given by the vectors

$$\mathbf{r}_{1(3)}^{(p)} = \pm \frac{a}{2} (1, 1, 0), \quad \mathbf{r}_{2(4)}^{(p)} = \pm \frac{a}{2} (-1, 1, 0).$$

Sites depicted as red dots on Fig 2(e), which are counted with a coefficient γ_1 in the constrainer definition, are lo-

cated at positions

$$\mathbf{r}_{5(9)}^{(p)} = \pm \frac{a}{2} (3, 1, 0), \quad \mathbf{r}_{6(10)}^{(p)} = \pm \frac{a}{2} (1, 3, 0),$$

$$\mathbf{r}_{7(11)}^{(p)} = \pm \frac{a}{2} (-1, 3, 0), \quad \mathbf{r}_{8(12)}^{(p)} = \pm \frac{a}{2} (-3, 1, 0).$$

Finally, the sites encapsulated in the constrainer definition (13), depicted by yellow dots on Fig 2(e), are sitting at positions

$$\mathbf{r}_{13(15)}^{(p)} = \pm \frac{a}{2} (3, 3, 0), \quad \mathbf{r}_{14(16)}^{(p)} = \pm \frac{a}{2} (-3, 3, 0).$$

The four sites located in the intermediate plane located above the parent system, depicted as green squares on Fig 2(e) are located at positions

$$\mathbf{r}_{1(3)}^{(l)} = (\pm a, 0, d), \quad \mathbf{r}_{2(4)}^{(l)} = (0, \pm a, d).$$

and with $-d$ as last component for sites located in the intermediate plane located below.

Appendix B: Definition of the structure factor – The structure factors depicted in the right panels of Fig. 2 are computed analytically using Henley’s projective method [27]; in the zero-temperature limit, the spin-spin correlation functions are expected to be proportional to the projector Π into the space orthogonal to the constraint vectors defined for each cluster following Eq. (2). For the two systems studied in the present work, there is a unique constraint vector and this projector is then simply equal to

$$\Pi = I - \mathbf{L} \frac{1}{\mathbf{L}^\dagger \mathbf{L}} \mathbf{L}^\dagger. \quad (15)$$

The structure factor can then be expressed, up to a multiplicative constant, as

$$\mathbb{S}(\mathbf{q}) \propto \sum_{m,p} \Pi_{mp} = n - 1 - \sum_{m \neq p} \frac{L_m(\mathbf{q}) \bar{L}_p(\mathbf{q})}{\|\mathbf{L}(\mathbf{q})\|^2} \quad (16)$$

where n is the number of \mathbf{L} components, that is, the number of sublattices, equal to 3 for the two systems studied in this work. $\bar{L}_p(\mathbf{q})$ denotes the complex conjugate of $L_p(\mathbf{q})$.

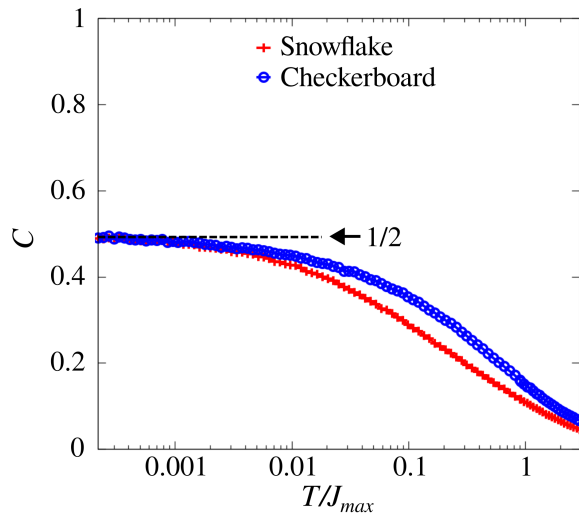


Figure 3. Specific heat per spin C as a function of temperature, computed through classical Monte Carlo simulations for both 3D lattices. The black arrow indicates that in both cases, the specific heat reaches a value of $C = 1/2$ at the lowest temperature ($T/J_{max} = 2 \times 10^{-4}$). These results have been obtained for a cluster of $N = 3 \times 15 \times 15 \times 10$ sites.

Appendix C: Monte Carlo simulations – To investigate the temperature-dependent behavior of the systems, we performed Monte Carlo simulations employing the Metropolis algorithm combined with overrelaxation techniques. The simulations were conducted within an annealing framework, where the temperature T was systematically reduced. All temperatures are expressed in units of the largest absolute value of the coupling constant, J_{max} , for each specific parameter set in the MC simula-

tions. For the 3D Checkerboard model, J_{max} in units of J (where J is the plaquette coupling constant) is defined as $J_{max} = 4\gamma_1 = 4$ for $\gamma_1 = 1$. This corresponds to the second-neighbor coupling introduced by γ_1 . For the 2D Snowflake model, where $\gamma = 1/2$, $J_{max} = 2 + 2\gamma = 3$. The systems were thermalized for a minimum of 10^6 MC steps, followed by 2×10^6 MC steps for calculating mean values. The system size N was defined as $N = n_s \times L_x \times L_x \times L_z$, where n_s represents the number of sites within the unit cell ($n_s = 3$ for both generalized snowflake honeycomb and checkerboard lattices). L_x and L_z denote the linear dimensions of the system, with $15 \leq L_x \leq 30$ and $10 \leq L_z \leq 20$.

To confirm the spin-liquid behavior of both 3D models, we computed two key quantities: the specific heat per spin C , given by $C = (\langle E^2 \rangle - \langle E \rangle^2) / NT^2$ where E is the energy of the system, and the static structure factor $\mathbb{S}(\mathbf{q})$, defined as $\mathbb{S}(\mathbf{q}) = \frac{1}{N} \sqrt{\langle |\sum_j \mathbf{S}_j e^{i\mathbf{q} \cdot \mathbf{r}_j}|^2 \rangle}$, whose corresponding plots are presented in the main text [Fig. 2].

Figure 3 shows the temperature dependence of the specific heat C for both the 3D snowflake and 3D generalized checkerboard models. In both cases, the specific heats monotonously increase upon cooling; there is no peak and thus no indication of any phase transition in both models. Furthermore, C reaches a plateau at a value of $C \simeq 1/2$ which is noticeably lower than the value of 1 traditionally expected for classical Heisenberg models. This is the signature of a large quantity of soft modes, consistent with an extensively vast ground state manifold [35, 36]. To further confirm the absence of magnetic order, we found no Bragg peaks in the structure factor of both models down to $T = 0.0002J_{max}$, as shown in the left panels of Figs. 2(b,c,d,f,g,h).